Chalcogenide Letters Vol. 14, No. 10, October 2017, p. 447 - 455

STRUCTURAL AND VIBRATIONAL PROPERTIES OF CHALCOPYRITE $CuGaTe_2$: A FIRST-PRINCIPLES STUDY

Y. YU*, Y.H. SHEN, J. DENG, X.L. ZHENG, G.D. ZHAO
College of Optoelectronic Technology, Chengdu University of Information Technology, Chengdu 610225, China

We present a first-principles study of the structural and vibrational properties for chalcopyrite semiconductor $CuGaTe_2$. The structural properties are calculated using a plane-wave pseudopotential method of density-functional theory. A linear-response method based on density-functional perturbation theory is used to derive the phonon dispersion curves. We calculate all zone-center phonon modes, identify Raman and infrared active modes, and report LO-TO splitting of the infrared modes. The results show an excellent agreement with experiment and propose several predictive behaviors.

(Received August 3, 2017; Accepted October 25, 2017)

Keywords: $CuGaTe_2$, DFPT, LO-TO splitting, vibrational properties

1. Introduction

The possibility of using I-III-VI_2 ternary chalcopyrite semiconductors for applications in optoelectronic devices has led to extensive investigation of the basic physical properties of these compounds in the three last decades. It is known that $CuGaTe_2$ has usually a *p*-type conductivity and a direct band gap E_g=1.22-1.24 eV at room temperature [1, 2]. This lies in the optimum range for solar energy conversion. Also, $CuGaTe_2$ is reported as an outstanding thermoelectric material [3]. However, it has been studied in less detail compared with other members of this family of ternaries.

Limited number of works on its structural [4-7], electrical [8-10], optical [8, 11, 12], thermoelectric [3, 7, 13, 14] and thermal [15-18] properties have been reported in the literature. This is probably due to the fact that preparation of large single crystals of $CuGaTe_2$, required for most experiments, is not easy [19]. The reported data on the lattice vibrational modes in this compound are also scarce. Experimentally, only four preliminary studies, one by infrared reflectivity (IR) [20] and three by Raman spectra [19, 21, 22], show measurements in the literature. Therefore, only a limited number of the vibrational modes are observed and no definite conclusion has been made about their possible symmetry. On the theoretical side, there have been only a few attempts to calculate the lattice dynamical and a detailed knowledge is still lacking. Only Zou et al. [23] investigated the lattice vibrational properties of $CuGaTe_2$ by linear-response method based on density-functional perturbation theory (DFPT) [24, 25]. However, the interesting effects of the longitudinal–optical/transverse-optical (LO-TO) splitting were not given and discussed. Modern first-principles calculation techniques of phonon crystal properties based on DFPT formalism have proven to be an effective research tool. The results of such investigations are highly reliable and have predictive power. Recently, first-principles calculations of lattice dynamics of chalcopyrite $CuInSe_2$ [26, 27], $CuGaS_2$ [28], $CuInS_2$ [29], $CuGaSe_2$ [30] and $ZnSnP_2$ [31] using DFPT have been reported.

The purpose of this paper is to obtain in more detail the dynamical properties of $CuGaTe_2$ using DFPT. Our calculations start with the structural optimization and check that our relaxed

*Corresponding author: yy2012@cuit.edu.cn

structural parameters are consistent with the experimental work. The phonon frequencies are then calculated from linear-response techniques. Finally, the LO-TO splittings are investigated. In the following, we describe the calculation methods and discuss the results.

2. Computational details

The present results have been obtained thanks to the use of the ABINIT code [32], which is based on density-functional theory (DFT) using the pseudopotential method and a plane-wave expansion of the wave functions. The interactions between the ions and valence electrons were described using norm-conserving local density approximation (LDA) pseudopotentials which are generated in the scheme of Troullier-Martins (TM) [33-35]. For the exchange-correlation potential we have used the LDA data of Ceperly-Alder, as parametrized by Perdew and Wang [36]. The Cu ($3d^{10}$, $4s^1$), Ga ($4s^2$, $4p^1$), and Te ($5s^2$, $5p^4$) orbital are treated as valence states.The pseudopotentials used in the present calculations are soft potentials of the TM type, available on the ABINIT web site. The density-functional perturbation theory is the basis of the linear-respond approach. Phonon frequencies and atoms displacements are obtained using the linear-respond method, which avoids the use of supercells and allows the calculation of dynamical matrix at arbitrary $\boldsymbol{q}$ vectors. Technical details of the computation of responses to strain perturbations, atoms displacements, and homogeneous electric fieldscan be found in Ref. 37 and 38, while Ref. 39 presents the subsequent computation of dynamical matrices.

The calculations were carried out with a 30hartree plane-wave energy cutoff, and the tetragonal Brillouin zone (BZ) was sampled with a regular and shifted 4×4×4 *k*-point mesh. Convergence tests show that the BZ sampling and the kinetic energy cutoff are sufficient to insure an excellent convergence within 1 cm^{-1} for the calculated phonon frequencies.

3. Results and discussion

3.1 Structural optimization

$CuGaTe_2$ is crystallized in the body-centered-tetragonal chalcopyrite structure with the space group $I\bar{4}2d$, and the structure of $CuGaTe_2$ is shown in Fig. 1.As is well known, the chalcopyrite structure of I-III-VI_2 semiconductors can be considered as derived from the well known cubic zinc-blende structure (space group T_d^2) by doubling the latter unit cell in the *z* direction and populating one of the face-centered cubic sublattice with group VI atoms and the other one with equal amounts of groups I and III atoms in a regular fashion. For $CuGaTe_2$, the Cu atom is located at (0, 0, 0), (0, 1/2, 1/4); Ga at (0, 0, 1/2), (0, 1/2, 3/4) and Te at (*u*, 1/4, 1/8), (-*u*, 3/4, 1/8), (3/4, *u*, 7/8), (1/4, -*u*, 7/8). Two unequal bond lengths $d_{\text{Cu-Te}}$ and $d_{\text{Ga-Te}}$ result in two structural deformations. First is characterized by *u* parameter defined as $u = 0.25 + \left(d_{Cu-Te}^2 - d_{Ga-Te}^2\right)/a^2$, where *a* is the lattice parameter in *x* and *y* direction.The second consequence of differing anion-cation bond lengths is a deformation of the unit cell along the *z* axis to a length *c* which is generally different from 2*a*. This tetragonal distortion is characterized by the quantity *c/a*.

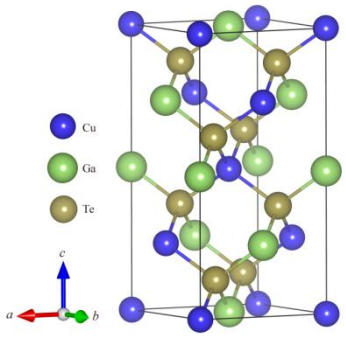

Fig. 1 Crystal structure of $CuGaTe_2$

Table 1. The equilibrium lattice constant a (c) (in Å), axial ratio c/a, cell volume V ($Å^3$) and internal parameter u for $CuGaTe_2$

Method	a	c	c/a	V	u
Present work (ABINIT-LDA)	5.916	11.774	1.990	412	0.234
Exp. (Ref. [40])	5.994	11.910	1.987	428	0.250
Exp. (Ref. [5])	6.023	11.940	1.982	433	0.256
CASTEP-GGA (Ref. [41])	6.109	12.180	1.994	455	—
WIEN2K-GGA (Ref. [42])	6.043	11.780	1.949	430	0.262
WIEN2K-GGA (Ref. [43])	6.105	12.126	1.986	452	0.244
VASP-LDA (Ref. [23])	5.950	11.780	1.980	417	—

The ground state structural properties are obtained by minimization of the total energy with respect to the unit cell volume. The calculations were carried out in the primitive cell of $CuGaTe_2$ containing two Cu, two Ga, and four Te atoms. The calculated lattice parameters, *a*, *c*/*a*, *V* and *u*, are compared to available experimental [5, 40] and calculated values [23, 41-43] in table 1. For $CuGaTe_2$, optimization of unit cell geometry within LDA leads to a = 5.916 Å, c = 11.774 Å. The calculated lattice constants are underestimated with the maximal error of 1.32%, which is typically the expected precision for the LDA. Considering the fact that the zero-point motion and thermal effects are not taken into account, the calculated lattice constant, tetragonal and tetrahedral distortion values agree with the experimental values quite well.The optimized results show our calculation method is feasible and we will adopt the optimized structure parameters to calculate vibrational properties.

3.2 Vibrational properties

A crystal lattice with *n* atoms per unit cell has 3*n* branches, three of which are acoustic and the remainder areoptical. There are 8 atoms in the primitive unit cell of $CuGaTe_2$, so there are 24 dispersion curves, which mean 24 normal vibration modes at the center Γ point. Based on the factor group theory, the reducible representations for the space group D_{2d}^{12} at the Γ point can be noted in Table 2.

Table 2 Character table for the D_{2d} point group (tetragonal)

$D_{2d}(\bar{4}2m)$	E	$2S_4$	C_2	$2C_2'$	$2\sigma_d$	Symmetry	Activity	Number	
								Optical	Acoustic
A_1 (Γ_1)	1	1	1	1	1	x^2+y^2, z^2	R	1	0
A_2 (Γ_2)	1	1	1	-1	-1	—	Silent	2	0
B_1 (Γ_3)	1	-1	1	1	-1	x^2-y^2	R	3	0
B_2 (Γ_4)	1	-1	1	-1	1	xy	R, IR	3	1
E (Γ_5)	2	0	-2	0	0	(x, y), (xz, yz)	R, IR	6	1

Group-theoreticalanalysis predicts the following irreducible representationfor acoustical and optical zone-center modes:

$$\Gamma_{aco} = 1B_2+1E,$$
$$\Gamma_{opt} = 1A_1+2A_2+3B_1+3B_2+6E.$$

This gives rise 21 optical phonon branches which at the center of the BZ decompose into one A_1 (Γ_1), two A_2 (Γ_2), three B_1 (Γ_3), three B_2 (Γ_4) and six E (Γ_5). All these modes, except the A_2, are Raman (R) active, whereas only B_2 and E modes are infrared (IR) active. Since the dipole moments of the B_2 modes are along the c axis and those of the E modes are in the plane perpendicular to this axis, polarized IR spectra will select the different symmetry modes. To make a comparison with phonons in III-V compounds it should be noted that in the latter case there is only one triply degenerateΓ_{15} mode at the center of the BZ but the use of the unit cell of the chalcopyrite folds the points of the BZ X(0, 0, $2\pi/a$), W($2\pi/a$, 0, π/a) and W(0, $2\pi/a$, π/a) into Γ in the chalcopyrite structure. The compatibility relations between the symmetry phonons in two crystal structures are shown in Fig. 2.

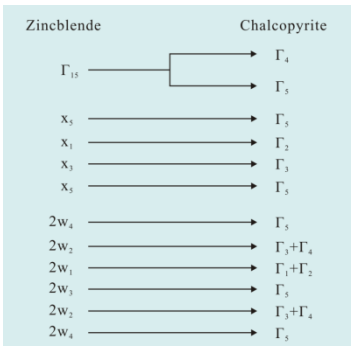

Fig. 2 Relationship between the symmetry of the modes in III-V compoundsand the corresponding zone-center optical modes in chalcopyrite compounds after folding

Positions of nonequivalent atoms are indicated in Fig. 3. There are four distinct Te, two Cu, and two Ga atoms.Locations of symmetry operators of the space group are given in the International Tables. Transformation properties of these atoms under symmetry operations of the space group are noted in Table 2, wherethe initial and transformed positions of distinct atoms are enclosed in parentheses.Using this information, the number of zone-center (Γ) vibrational modes belonging to a particular symmetry type can be calculated. Symmetry coordinates for the onefold

A and *B* representations are given in Fig. 3 and 4, respectively, and for the twofold *E* representations in Fig. 5. A detailed discussion can be found in Ref. 44.

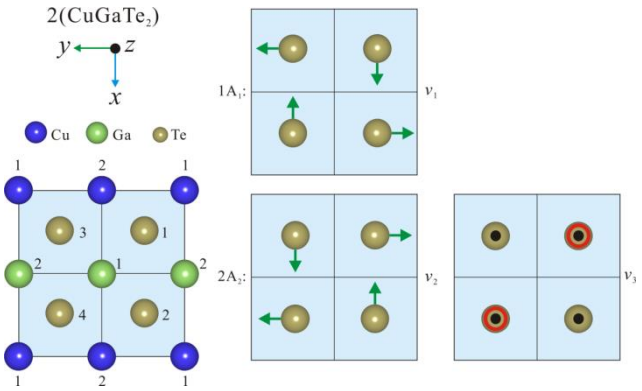

Fig. 3 (001) projection of unit cell showing positions of four nonequivalent Te atoms, the two nonequivalent Cu atoms and the two nonequivalent Ga atoms. Symmetry coordinates for A modes ($1A_1$+$2A_2$); displacements in the xy plane are represented byarrows and displacements in the z direction by open and closed circles.

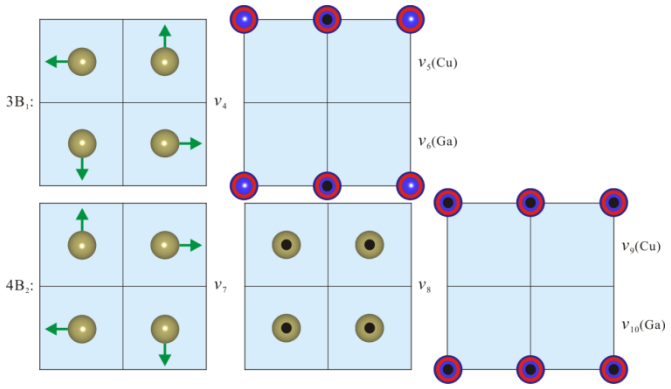

Fig. 4 Symmetry coordinates for B modes ($3B_1$+$4B_2$); displacements in the xy plane are represented by arrows and displacements in the z direction by open and closed circles

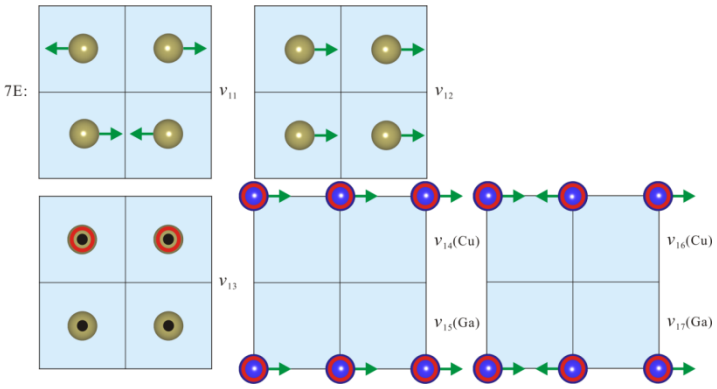

Fig. 5. Symmetry coordinates for E modes (7E); displacements in the xy plane are represented by arrows and displacements in the z direction by open and closed circles

Complete phonon branches of $CuGaTe_2$ are plotted for the high-symmetry lines in the BZ together with the corresponding phonon density of states (DOS) in Fig. 6. The phonon DOS is normalized to the number of phonons. Interesting feature of acoustic branches around the Γ point is observed, especially along Γ-X and Γ-Z directions. In order to obtain the phonon dispersion curves throughout the BZ, the dynamical matrices are obtained 4×4×4 grid of *q* points, and real space force constants are then found by Fourier transform of the dynamical matrices [45]. The acoustic sum rule is applied to force the three acoustic phonon frequencies at the Γ point equal to zero strictly as being implied by translation symmetry. In Table 3, the calculated zone-center phonon frequencies for $CuGaTe_2$ are presented as well as the experimental [19-22] and theoretical [23] values in the literature. As shown in Fig. 6 and Table 3, the zone-center phonon spectra of $CuGaTe_2$ consist of three groups. The low frequency group of modes has a range of values from 58 to 155 cm^{-1} and the medium frequency group of modes has a range of values from 160 to 194 cm^{-1}. The highest frequency group of modes can be up to 211 cm^{-1}. Unfortunately, some vibration modes have not been observed in previous experiments, including infrared [20] and Raman measurements [19, 21, 22].

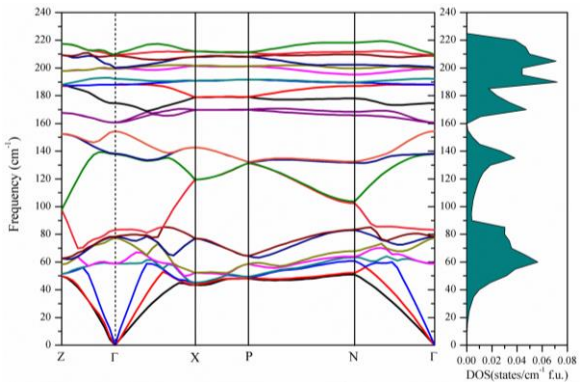

Fig. 6 Calculated phonon dispersion curves along symmetry lines in the BZ and the corresponding phonon density of states (DOS) for $CuGaTe_2$

As there is only one totally symmetric A_1 mode, it is uniquely determined and corresponds to variation of the internal coordinate *u*(Te). Our calculated value for A_1 mode is 138.2 cm^{-1} which is in good agreement with the experimental and theory values. It should be noted that the group-theoretical analysis forbids the appearance of vibrations of symmetry A_2 in Raman spectra of ideal crystals with a chalcopyrite lattice. However, it seems that A_2 mode are reported to be activated in Raman spectra [19, 22]. This is because the prohibition can be removed in the case of a defect structure and additional scattering will result in the activation of the A_2 mode [46]. As shown in Table 3, our calculated frequencies and Raman measurements reported by Ref. 19 coupled with the results of experimental as well as computational studies on other Cu-based chalcopyrites seem to indicate thateach one of three B_1 mode frequencies is in low, mediun, and high frequency region.

Inclusion of the long range polarization interaction results in splitting of the B_2 and *E* modes into LO and TO components. It should be noted that the linear-response method was performed to calculate the phonon frequencies of $CuGaTe_2$ by Zou *et al*. [23]. Although the calculated frequencies show a better agreement with ours, the LO-TO splittings are not given and discussed. The splitting depends on the effective charges and dielectric tensors of the system which are directly accessible to the linear-respond method in our work. The LO-TO splittings for B_2 and *E* modes are presented in Table 3 and the values agree well the experimental results [19-21]. For $CuGaTe_2$, the LO-TO splitting is small. The splitting is even zero in the low frequency region, because the low frequency modes are essentially the folded acoustic modes, they correspond to whole molecular units moving relative to each other. Moreover, it should be note that one of the mode *E* (211.1 cm^{-1}) calculated in our work is quite different from the experimental data (269 cm^{-1},

272 cm^{-1}, or 274 cm^{-1}). The calculated result is consistent with Zou's data (210.5 cm^{-1}) [23] which is calculated by the same method. The difference between the theoretical and experimental data may be due to the defects and disorder in the experimental structure, and a detailed discussion can be found in Ref. 46. Overall, the calculated zone-center phonon frequencies for $CuGaTe_2$ are in agreement with experimental data as shown in Table 3.

Table 3 A comparison of calculated phonon frequencies (in cm^{-1}) at the Γ point with Raman and infrared data as well as with other theory values. Two numbers in a row correspond to LO/TO frequencies

Mode		Theory	Theory	Experiment			
		Present	Ab initio[23]	R[22]	R[19]	R[21]	IR[20]
A_1	R	138.2	139.2	136	135	138	—
A_2	Silent	137.7	138.0	122	117	—	—
	Silent	154.4	160.2	—	—	—	—
B_1	R	83.2	76.2	—	64	—	—
	R	174.6	155.4	148	148	—	—
	R	209.0	186.8	185	190	—	—
B_2	R, IR	77.4/77.4	76.6	—	70	—	72
	R, IR	192.1/193.1	190.1	205	204	203	200
	R, IR	200.2/202.2	209.8	226	224	223	—
E	R, IR	58.8/58.8	57.7	74	54	—	—
	R, IR	78.3/78.3	81.8	79	76	76	72
	R, IR	160.6/160.6	173.3	173	170	167	166
	R, IR	187.9/188.3	201.1	213	211	211	209
	R, IR	199.5/200.2	201.2	—	220	—	—
	R, IR	209.6/211.1	210.5	269	272	274	—

4. Conclusions

We have investigated the structural and vibrational properties of chalcopyrite $CuGaTe_2$ within linear-response method based on density-functional perturbation theory. First of all, the optimal ground state structure is studied within the LDA approaches. The structural parameters, including the internal coordinates, are relaxed, and excellent agreement is achieved with experimental results. And then, the phonon frequencies at the Γ point of the BZ are calculated and their assignments are given. The LO-TO splittings for B_2 and E modes are presented and the values of LO-TO splitting agree well the infrared and Raman measurements. We believe that our theoretical predictions should be highly valuable for the experimental community in framework of the characterization of $CuGaTe_2$.

Acknowledgments

This work was supported by the Open Research Fund of Computational Physics Key Laboratory of Sichuan Province, Yibin University (Grant No. JSWL2014KFZ01), Scientific Research Fund of Sichuan Provincial Education Department (Grant No. 16ZB0209), Scientific Research Foundation of Chengdu University of Information Technology (Grant No. J201611), and National Natural Science Foundation of China (Grant No. 11547224).

References

[1] G. Marin, G.S. Perez, G. Marcano, S.M. Wasim, C. Rincon, J. Phys. Chem. Solids **64,**1869 (2003).
[2] S.A.A. Elhady, B.A. Mansour, S.H. Moustafa, Phys. Status Solidi A **149,** 601 (1995).
[3] T. Plirdpring, K. Kurosaki, A. Kosuga, T. Day, S. Firdosy, V. Ravi, G.J. Snyder, A. Harnwunggmoung, T. Sugahara, Y. Ohishi, H. Muta, S. Yamanaka, Adv. Mater. **24,** 3622 (2012).
[4] B. Grzeta-Plenkovic, B. Santic, J. Appl. Cryst. **16,** 576 (1983).
[5] M. Leon, J.M. Merino, J.L.M.D. Vidales, J. Mater. Sci. **27,** 4495 (1992).
[6] Y.T. Qin, P.F. Qiu, R.H. Liu, Y.L. Li, F. Hao, T.S. Zhang, D.D. Ren, X. Shi, L.D. Chen, J. Mater.Chem.A **4,**1277 (2016).
[7] W.C. Wu, Y.P. Li, Z.L. Du, Q.S. Meng, Z. Sun, W. Ren, J.L. Cui, Appl. Phys. Lett. **103,** 011905 (2013).
[8] A. Messous, A. Bouloufa, K. Djessas, I. Bouchama, Phys. Status Solidi C **11,** 1443 (2014).
[9] H. Neumann, D. Peters, B. Schumann, G. Kuhn, Phys. Status Solidi A **52,** 559 (1979).
[10] B. Santic, Phys. Status Solidi A **133,** 137 (1992).
[11] J. Krustov, H. Collan, K. Hjelt, M. Yakushev, A.E. Hill, R.D. Tomlinson, H. Mandar, H. Neumann, J. Appl. Phys. **83,** 7867 (1998).
[12] J. Krustov, J. Raudoja, M. Yakushev, R.D. Pilkington, H. Collan, J. Appl. Phys. **86,** 5305 (1999).
[13] V.K. Gudelli, V. Kanchana, G. Vaitheeswaran, A. Svane, N.E. Christensen, J. Appl. Phys. **114,** 223707 (2013).
[14] J.L. Cui, Y.P. Li, Z.L. Du, Q.S. Meng, H. Zhou, J. Mater. Chem. A **1,** 677 (2013).
[15] B. Kuhn, W. Kaefer, F. Fess, K. Friemelt, C. Turner, M. Wendl, E. Bucher, Phys. Status Solidi A **162,** 661 (1997).
[16] S.M. Wasim, G. Marcano, G.S. Porras, Jpn J. Appl. Phys. **19,** 133 (1980).
[17] K. Bohmhammel, P. Deus, G. Kuhn, W. Moller, Phys. Status Solidi A **71,** 505 (1982).
[18] I.V. Bodnar, N.S. Orlova, Cryst. Res. Technol. **21,** 1091 (1986).
[19] C. Rincon, S.M. Wasim, G. Marin, E. Hernandez, J. Galibert, J. Phys. Chem. Solids **62,** 847 (2001).
[20] V. Riede, H. Sobotta, H. Neumann, H.X. Nguyen, W. Moller, G. Kuhn, Solid State Comm. **28,** 449 (1978).
[21] C. Rincon, S.M. Wasim, G. Marin, J.R. Huntzinger, J. Galibert, A. Zwick, Mater. Lett. **38,** 305 (1999).
[22] S. Kesari, N.P. Salke, R. Rao, Dae Solid State Physics Symposium **1731,** 847 (2016).
[23] D.F. Zou, S.H. Xie, Y.Y. Liu, J.G. Lin, J.Y. Li, J. Alloy. Compd. **570,** 150 (2013).
[24] S. Baroni, P. Giannozzi, A. Testa, Phys. Rev. Lett. **58,** 1861 (1987).
[25] S. Baroni S. de Gironcoli, A. Dal Corso, P. Giannozzi, Rev. Mod. Phys. **73,** 515 (2001).
[26] J. Lazewski, K. Parlinski, B. Hennion, R. Fouret, J. Phys.: Condens. Matter **11,** 9665 (1999).
[27] Y. Yu, G.D. Zhao, X.L. Zheng, Z.R. Wei, Chalcogenide Lett. **13,** 15 (2016).
[28] M. Akdogan, R. Eryigit, J. Phys:Condens. Matter **14,** 7493 (2002).
[29] R. Eryigit, C. Parlak, R. Erygit, Eur. Phys. J. B **33,** 251 (2003).
[30] C. Parlak, R. Eryigit, Phys. Rev. B **73,** 245217 (2006).
[31] Y. Yu, Y.J. Dong, Y.H. Shen, G.D. Zhao, X.L. Zheng, J.N. Sheng, Chin. Phys. B **26,** 046302 (2017).
[32] X. Gonze, J.-M.Beuken, R. Caracas, F. Detraux, M. Fuchs, G.-M. Rignanese, L. Sindic, M. Verstraete, G. Zerah, F. Jollet, M. Torrent, A. Roy, M. Mikami, Ph. Ghosez, J.-Y. Raty, D.C. Allan, Comput. Mater.Sci. **25,** 478 (2002). http://www.abinit.org.
[33] M.C. Payne, M.P. Teter, D.C. Allan, T.A. Arias, J.D. Joannopoulos, Rev. Mod. Phys. **64,** 1045 (1992).
[34] X. Gonze, Phys. Rev. B **54,** 4383 (1996).
[35] M. Fuchs, M. Scheffler, Comput. Phys. Commun. **119,** 67 (1999).

[36] J.P. Perdew, Y. Wang, Phys. Rev. B **45,** 13244 (1992).
[37] X. Gonze, Phys. Rev. B **55,** 10337 (1997).
[38] D.R. Hamann, X. Wu, K.M. Rabe, D. Vanderbilt, Phys. Rev. B**71,** 035117 (2005).
[39] X. Gonze, C. Lee, Phys. Rev. B **55,** 10355 (1997).
[40] J.E. Jaffe, A. Zunger, Phys. Rev. B **29**, 1882 (1984).
[41] X.Z. Zhang, K.S. Shen, Z.Y. Jiao, X.F. Huang, Comput. Theor.Chem. **1010,** 67 (2013).
[42] P. Singh, S. Sharma, S. Kumari, V.K. Saraswat, D. Sharma, A.S. Verma, Semiconductors **51,** 679 (2017).
[43] L. Xue, B. Xu, D.G. Zhao, L. Yi, Comp. Mater. Sci. **90,** 143 (2014).
[44] I.P. Kaminow, E. Buehler, J.H. Wernick, Phys. Rev. B **2,** 960 (1970).
[45] S. Goedecker, SIAM J. Sci. Comput.(USA) **18,** 1605 (1997).
[46] A.V. Kopytov, A.V. Kosobutsky, Phys. Solid State **51,** 2115 (2009).